

Analysis of wing in ground-craft water landing

Marek Roškowicz¹, Ryszard Chachurski¹, Łukasz Omen¹, Michał Jędrak¹ 

¹ Faculty of Mechatronics, Armament and Aerospace, Military University of Technology, ul. Sylwester Kaliski 2, 00-908 Warsaw, Poland

* Corresponding author's e-mail: michal.jedrak@wat.edu.pl

ABSTRACT

Unmanned aerial platforms, along with surface platforms, can be elements of rapid response force systems at sea. The unmanned surface vehicle (USV), unmanned aerial vehicle (UAV), wing in ground (WIG) platform is a type of vehicle that combines the features of an aircraft and a surface vehicle. In its operational range, it moves using the so-called ground effect. This phenomenon consists in increasing the lift of an aircraft moving at a small height above the ground or water (the height is assumed to be half the wing span). To consider this problem, we first prepared a computational task for the impact of a ball, box, and cylinder-shaped bodies on water. The calculations were carried out using the finite element method using the capabilities of the LS-DYNA environment. Computer simulations of impact of the those shaped bodies on water were experimentally verified using the so-called high-speed camera and the image analysis system. Second, analytical calculations and numerical simulations of the launch of an example USV-UAV-WIG structure were carried out. For the purposes of the analyses, a numerical model of the structure and a model of the water-solid interaction were prepared. On the basis of the results of the calculations obtained, the loads occurring during landing of the vehicle were defined.

Keywords: finite element method, aircraft engineering, UAV, wing-in-ground effect, fluid structure interference.

INTRODUCTION

The problems of interactions occurring at the fluid-solid interface are challenges in the analysis of various technical solutions, including those related to the motion of a torpedo, fluid flow in a power turbine, fluid interactions in pump structural elements, or aircraft take-off and landing operations on water. Such interactions are related, among others, to the change in free surfaces and the occurrence of a strong coupling between the fluid and the solid [1].

The search for solutions in the area of fluid-solid interactions can be carried out on the basis of theoretical considerations, experimental studies, or numerical simulations [2–5]. Theoretical analyses are usually based on linear or weakly non-linear fluid dynamics. The problem of interaction between fluids and solids was dealt with by, among others, Von Karman (1929), who developed the first theory concerning this type of

problem. He was the first to propose an analytical method to estimate the forces of impact of a wedge-shaped body on water and introduced a method to determine landing loads on water for seaplanes [6]. Then he carried out a series of analyses related to the interaction of water with solids based on a theoretical approach, also supported by experimental tests. Most of the later works in the early period were based on this theory.

Experimental studies in this area are generally expensive and in many cases the physical model cannot be scaled to a practical experimental model [7]. However, for structures that are crucial to human safety, expensive experimental validation tests are also carried out.

The solution to the problem of searching for reactions between two media and at the same time avoiding the problem of performing expensive experimental studies is to use modern computational tools designed to perform numerical simulations in the area of dynamics. In the work [8] it

was indicated that numerical analysis should be treated as the main research tool for the analysis of the dynamic interaction of two media, and accurate numerical models of fluid-solid interactions can replace expensive and time-consuming experimental studies. In recent decades, numerical simulations based on smoothed particle hydrodynamics (SPH) and arbitrary Lagrangian-Eulerian (ALE) methods [9–10] have been used to solve dynamic problems of fluid-solid interactions. The SPH method is a meshless method that uses the Lagrangian equation to describe the material structure, while the ALE method based on finite elements can use both the Lagrangian formula for the analysis of solids and the Eulerian formula for the analysis of fluids.

The meshless SPH method allows modeling phenomena with very large deformations, which in the case of mesh methods causes distortions and mesh entanglements. However, this type of advantage of the method is associated with the need to use large computational resources; hence, the calculations performed with this method are associated with high costs. Taking into account the criterion of potential resources necessary to perform

the calculations, the ALE method is less demanding. Additionally, the method allows for any displacement of the fluid domain with respect to the material or spatial description. In this way, a large deformation is associated with a fluid moving fluid boundary [11]. The SPH method was developed by Gingold, Monaghan, and Lucy in 1977, initially for astrophysical problems. It is currently used in many fields of research, including astrophysics, ballistics, volcanology, and oceanography.

The ALE method was developed by Hirt and Nichols in 1981 and was initially used in flow calculations. In later years, it was applied to fluid-solid interaction problems [12].

In the work [13] the LS DYNA software was used for the first time as a computational tool to simulate the impact of a spacecraft, the Apollo 15 lunar module – on water (Fig. 1). The simulation results were verified by comparing them with the results of the experimental tests, but the response of the structure after the simulated time of 30–40 ms was not very satisfactory. The fluid field was simulated as a kind of solid, which caused computational problems related to significant distortions of the computational mesh

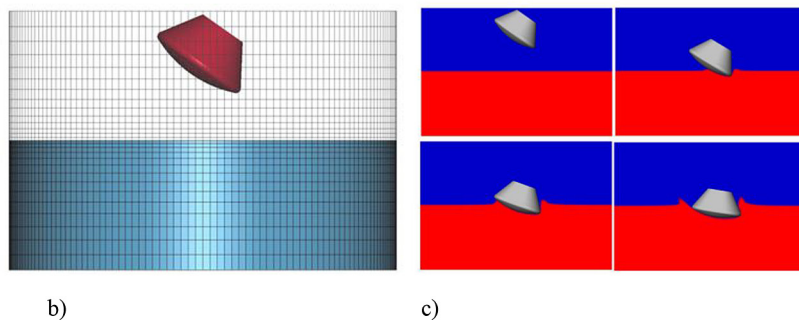
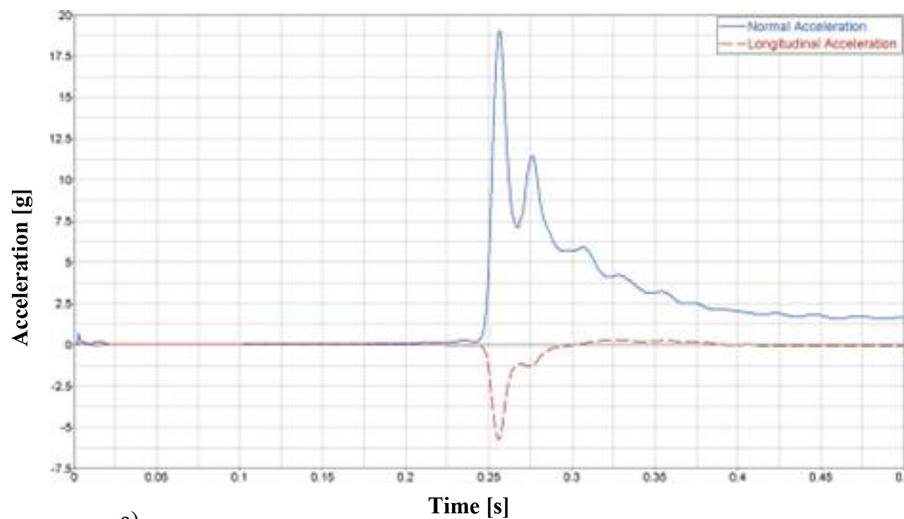


Figure 1. Results presented in the paper [13] a) acceleration graphs over time, b), FEM model, c) qualitative results

due to large fluid deformations. In the following years, with the development of the Arbitrary Lagrange-Euler (ALE) method [14–15], an improved computational environment was used to simulate the characteristics of spacecraft landing on water, where the fluid field was defined by ALE elements. Comparison of experimental data with the results of numerical simulations confirmed the usefulness of numerical simulations performed in this way.

Comparative analyzes were also performed using computational tools using mesh and meshless methods to solve problems. For example, in [16], a comparison of the SPH and ALE methods was presented in relation to the vertical drop of a fuselage section from a passenger plane into the water (Fig. 2). The aim of the tests and calculations was to assess the energy absorption capacity of the composite sandwich structure (honeycomb system) in the event of its impact with the water. The results of the experimental tests were used to validate the model. The work also showed that the ALE method provides good agreement between the numerical and experimental results. For the SPH method, additional calculations were performed to assess the

geometry of the effect of the particle system on the obtained results (Fig. 3). As a result of the analyzes, it was found that the best correlation exists for a particle spacing of 1.5 inches.

In [17], the vertical impact of a composite fuselage section on soft ground and water was analyzed to investigate the effect of energy absorbers on the reaction that occurs in the hull structure. Additionally, a full-scale experiment was performed in the work to validate the numerical models (Fig. 4). The tests showed good agreement between the numerical calculation results and the experimental results. It was found that the concept of a sandwich structure core in the form of compressed honeycomb cylinders can be an effective damper of dynamic loads.

Interactions between water and solids in aircraft structures concern not only special cases related to aircraft incidents/accidents, but also to the operational use of aircraft. Examples of this type of use of aircraft structures are seaplanes or screen planes. When defining loads occurring during the use of such structures operating on the boundary of two media, that is, liquid and gas (air), the water landing operation is one of the important stages of analyzes related to defining the

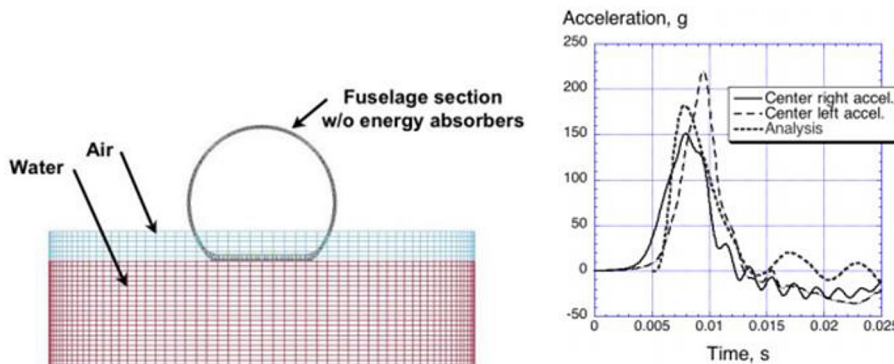


Figure 2. ALE model results from [16]

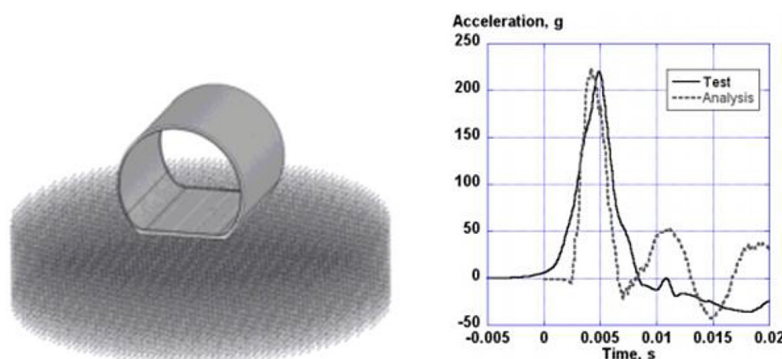


Figure 3. SPH model results from [16]

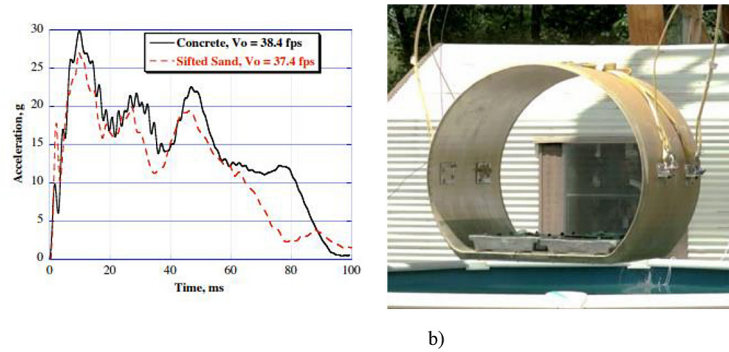


Figure 4. Results presented in the paper [17] a) acceleration time responses for concrete and soft soil surface impact, b) fuselage section

effort of the structure. When performing strength calculations, it is assumed that the maximum operational loads occur during the water landing operation [18]. The issue of maximum loads during water landing particularly concerns objects using the so-called ground effect occurring during the movement of aircraft (screen planes) at a very low height above the water surface - equal to approximately 0.3 of the aerodynamic chord of the airfoil. Numerous publications [19–20] have demonstrated the positive influence of the ground effect, for example, by shortening the runway of the screen plane and increasing safety during flight and landing. There is also a positive effect of this phenomenon on the specific fuel consumption of the screen plane power unit.

During the ditching operation, on the one hand, the horizontal component of the velocity vector should be as small as possible, among others to eliminate negative dynamic interactions, on the other hand, the aircraft must also maintain its basic aerodynamic characteristics during the ditching in order to be a fully controllable object [21]. The strains of the aircraft structural elements during the landing operation should be elastic, and even if there are areas of the aircraft structure skin that undergo local buckling, these should be strains in the elastic range. To define the loads occurring during landing in the semimonocoque elements of the aircraft structure, the problem of fluid-solid interaction should be solved.

In this paper, an attempt was made to estimate the loads that occur in the structure of an unmanned aerial vehicle (WIG-craft) made of two different materials (composite and metal) during its water landing. Since the task of estimating the loads occurring during landing in an aircraft structure with the following dimensions: span 6 m., length 5.6 m and total weight 148 kg for composite structure,

and 234 kg for metal structure, is a time-consuming and energy-intensive task in the context of the performance of currently used workstations, first calculations and experimental verification tests were performed for the case of a different solid bodies in the shape of a ball, box, and cylinder, all of them made by different materials, hitting water. For the calculations of this simplified case, two calculation methods occurring in the LS DYNA computational environment were used: SPH and ALE. Based on the results obtained, the calculation method for landing an unmanned aerial vehicle (screen plane) on water was selected, and the state of the structure's effort was defined.

SPH AND ALE METHOD

The SPH and ALE methods are currently widely used in numerical calculations of interactions occurring at the fluid-solid interface. The SPH method has gained popularity because of its computational stability and the ability to solve strongly nonlinear problems.

Smoothed particle hydrodynamics (SPH) is based on the N-body interaction scheme. The method was developed to avoid the limitations of mesh entanglement, which occur in the case of extreme deformation problems in the finite element method. The main difference between classical methods and SPH is the lack of a mesh. Therefore, particles are the basis for calculations, and the defined equations are solved on their basis. In the own analyses, the SPH model was also used to simulate the problem of water-structure interaction of an aircraft. The basic equation of the following SPH method is the relationship:

$$\frac{d\rho}{dt} = -\rho \nabla v \quad (1)$$

$$\frac{dv}{dt} = -\frac{1}{\rho} \nabla \rho + \frac{\mu}{\rho} \nabla^2 v + g + \frac{1}{\rho} \nabla(\rho R) \quad (2)$$

where: ρ – fluid density; v – velocity vector; μ – dynamic viscosity; g – acceleration of gravity; R – Reynolds stress tensor.

To solve the equations of motion, the technique of artificial fluid compressibility is used:

$$p = C_0^2(\rho - \rho_0) \quad (3)$$

where: p – pressure; ρ_0 – initial fluid density; ρ – fluid density; C_0 – speed of sound.

The approximation of the particle field function and its derivatives can be written as:

$$\frac{d\rho_i}{dt} = \sum_{j=1}^N m_j v_{ij} \nabla_i W_{ij} \quad (4)$$

$$\begin{aligned} \frac{dv_i}{dt} = & -\sum_{j=1}^N m_j \left(\frac{p_i}{\rho_i^2} + \frac{p_j}{\rho_j^2} \right) \nabla_i W_{ij} + \\ & + \sum_{j=1}^N \frac{4m_j(\mu_i + \mu_j)x_{ij} \nabla_i W_{ij}}{(\rho_i + \rho_j)^2 (x_{ij}^2 + 0,01h^2)} v_{ij} + \\ & + \sum_a^n m_b \left(\frac{R_a}{\rho_a} + \frac{R_b}{\rho_b} \right) \nabla_a W_{ab} + g \end{aligned} \quad (5)$$

where: ∇ – nabla; m – mass; ρ – density; v – velocity vector; W – Kernel function; p – pressure; μ – dynamic viscosity; x – x coordinate of the particle; h – particle smoothing length; i, j – particle numbering; a, b – numbering of spatial dimensions.

The SPH equations for the motion of a rigid body take the form:

$$\frac{du_0}{dt} = \frac{\sum m_j a_j}{M} + g \quad (6)$$

$$\frac{d\omega_0}{dt} = \frac{\sum m_j (r_j - R_0) \times a_j}{I_0} \quad (7)$$

where: u_0 – resultant velocity of the center of mass; r_j – distance of the center of mass from the axis of rotation; I_0 – moment of inertia; M – mass of the entire object; m – mass of a single particle; a – acceleration; ω_0 – angular velocity; R_0 – particle radius; t – time; j – particle number.

In turn, the ALE method perfectly combines the advantages of the Lagrange and Eulerian methods in such a way that if as a result of the change individual subregions of the network obtain unfavorable geometry, the nodes of the element will be moved to such an extent as to avoid

the formation of a numerically unstable network. The method has the advantage over other adaptive methods that both the number of nodes and the number of elements are preserved. In the ALE method, the mesh movement is independent of the material and space by introducing a reference coordinate system, which not only solves the problem of large deformations described by Lagrange, but also solves the problem of tracking the coupling described by Eulerian. The ALE method in the LS-DYNA code is a computational algorithm using momentum conservation equations. Energy, mass, and momentum are conserved and transferred from element to element. LS-DYNA uses the element division technique to solve the conservation equations using the Eulerian and ALE formulas. The principles of conservation of mass, momentum and energy are expressed by the following equations:

$$\frac{\partial \rho}{\partial t} + m_c \nabla \rho = -\rho \nabla u \quad (8)$$

$$\rho \frac{\partial u}{\partial t} + \rho m_c \nabla u = -\nabla p \quad (9)$$

$$\rho \frac{\partial e}{\partial t} + \rho m_c \nabla e = -\nabla(fu) \quad (10)$$

where: ∇ – nabla; u – resultant fluid velocity; m_c – fluid convection velocity; t – time; ρ – density of the medium; e – energy per unit mass; f – external load.

The penalty function method is chosen to process the coupling at the fluid-solid interface, which is equivalent to defining a series of damping spring systems between the fluid and the structural nodes. The coupling force F is a function of the relative displacement and relative velocity, as shown in the equation:

$$F = kd + cd \quad (11)$$

where: k and c are the stiffness and damping coefficients, respectively, and d is the penetration depth.

In LS-DYNA, the constitutive model and the equation of state are used simultaneously to describe the fluid material. The material property of the fluid is defined by the material model *MAT_NULL. The relationship between pressure and volume of water and air is defined by the linear polynomial equation of state:

$$p = C_0 + C_1 \mu_\rho + C_2 \mu_\rho^2 + C_3 \mu_\rho^3 + (b_0 + b_1 \mu_\rho + b_2 \mu_\rho^2) E \quad (12)$$

where: μ_p – density change rate; p – pressure; E – energy per unit volume; C , b – material constants.

Using the ALE formulation, the structure is modeled using a Lagrangian mesh of deformable elements with associated nodes that move with the element. A fluid (e.g. water) is typically modelled using a stationary Eulerian mesh in which the fluid material flows while conserving mass, momentum, and energy. When using the ALE algorithm, a portion of the air volume above the water must also be modeled using an Eulerian mesh to allow for the generation and movement of waves, thus simulating water deformations such as splashing water. In LS-DYNA, the coupling of Lagrangian and Eulerian meshes to solve the fluid-structure interaction problem is defined using the *CONSTRAINED_LAGRANGE_IN_SOLID tab.

CASE OF A BALL, BOX, AND CYLINDER HITTING THE WATER

In order to compare the results obtained using two calculation methods, i.e. the SPH and ALE methods, an analysis of the impact of the ball, box, and cylinder on water was performed. The results of the obtained simulations were compared with the experimental tests. The LS DYNA environment was used to calculate this simplified case. The boundary conditions of the simulations performed were the same as those of the experiment conducted in the next stage.

A model of a vessel with water was prepared in the form of a cylindrical shell with a height of 370 mm and a diameter of 45 mm, 1 mm thick, which corresponded to the geometry of the vessel used in the experiment. The MAT*ELASTIC card was used to model the cylindrical shell, where the material properties of the steel were defined ($E = 210$ GPa, $\rho = 7800$ kg/m³, $\nu = 0.33$). A model of a sphere with a diameter of 30 mm was prepared using 45 solid elements, the box model had dimensions of 33 mm × 11 mm × 11 mm and had 40 solid elements, while the diameter of the cylinder was 30 mm and height of 10 mm, modeled using 35 solid elements. The material properties of all of those bodies was modeled using the MAT*RIGID card, where the material properties of the sphere were defined as the properties of rubber, box as wood, cylinder as high-density PE. The same models for all bodies were used in both the SPH and

ALE calculations. Calculations were made for a free fall of a body into water placed 130 mm above the water surface. Depending on the method, water was modeled in two ways: in the SPH method using 8000 particles, while in the ALE method using 90 thousand elements. The height of the liquid column in the vessel (from its base) assumed for the calculations was 240 mm. The dynamic system of the bodies falling into the water assumed for calculations is shown in Figure 5.

The *MAT_NULL card and the *EOS_LINEAR_POLYNOMIAL equation of state were used to define the water properties in both models, and the exact parameters were taken from [22]. The input data are presented in Table 1.

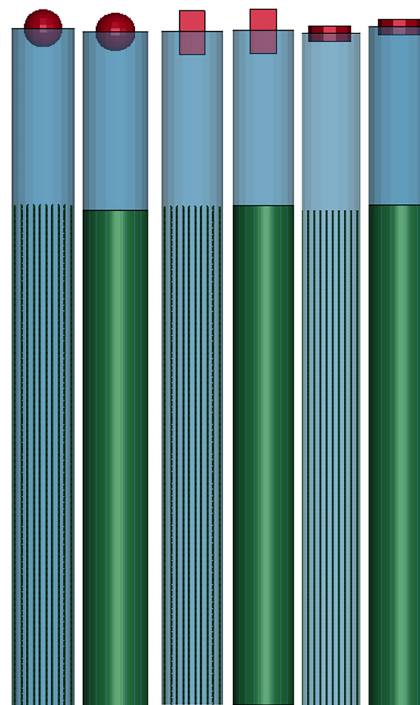


Figure 5. Position of ball, box, cylinder and vessel with water for time $t = 0$ s

Table 1. Material data of water [22]

*MAT_NULL	
Density [kg/m ³]	1000
*EOS_LINEAR_POLYNOMIAL	
C_0 [Pa]	0
C_1 [Pa]	2 000 000 000
C_2 [Pa]	8 430 000 000
C_3 [Pa]	8 010 000 000
b_0	0.44
b_1	1.39
b_2	0

The density data for the bodies are presented in Table 2. The water vessel boundary conditions included the condition that the vessel was not moving using the following condition of fixing the bottom of the vessel ($T_x = 0, T_y = 0, T_z = 0, R_x = 0, R_y = 0, R_z = 0$). For the bodies, the gravitational acceleration effect was defined as $g = 9.806 \text{ m/s}^2$.

In the SPH method, the *AUTOMATIC_NODES_TO_SURFACE card was used to define the interaction and simulate the impact of the bodies on the water. This is a type of contact that takes into account the interaction of the nodes in the water model with the solid elements of the bodies. Additionally, the interaction of water with the vessel walls was taken into account through the same card, as well as any contact between the vessel wall and the bodies through the *AUTOMATIC_SURFACE_TO_SURFACE card. The end of the calculations was set at 215 ms, which resulted from the measurements made in the next stage using the so-called high-speed camera, when the ball, or box, or cylinder speed in the water was 0 m/s. It was assumed that the immersion results of the calculations of the maximum depth of body immersion in water were assumed to be compared with the results of the experimental tests.

Experimental tests, to verify the results of numerical simulations, consisted of repeatedly dropping a rubber ball into a cylindrical vessel filled with a column of liquid 240 mm high from its base with water and observing the phenomenon of the body collision with water using a high-speed Chronos 14–1.0 camera (Canada). The image was recorded as a monochrome image at a frequency of one thousand frames per second at a resolution of 1280×1024 pixels.

An example comparison of the results of numerical simulations performed using the SPH method with images recorded with a high-speed camera is presented in Figure 6. The time to the bodies impact with the water was 163 ms.

Qualitative assessment indicates that the numerical simulations match the behavior of the fluid after the impact of the ball and box, but in the case of cylinder behaviour of the fluid is different in the simulation and experiment. This is due to the fact

Table 2. Density data of the ball, box, and cylinder

Density [kg/m ³]	
Ball	813
Box	671
Cylinder	965

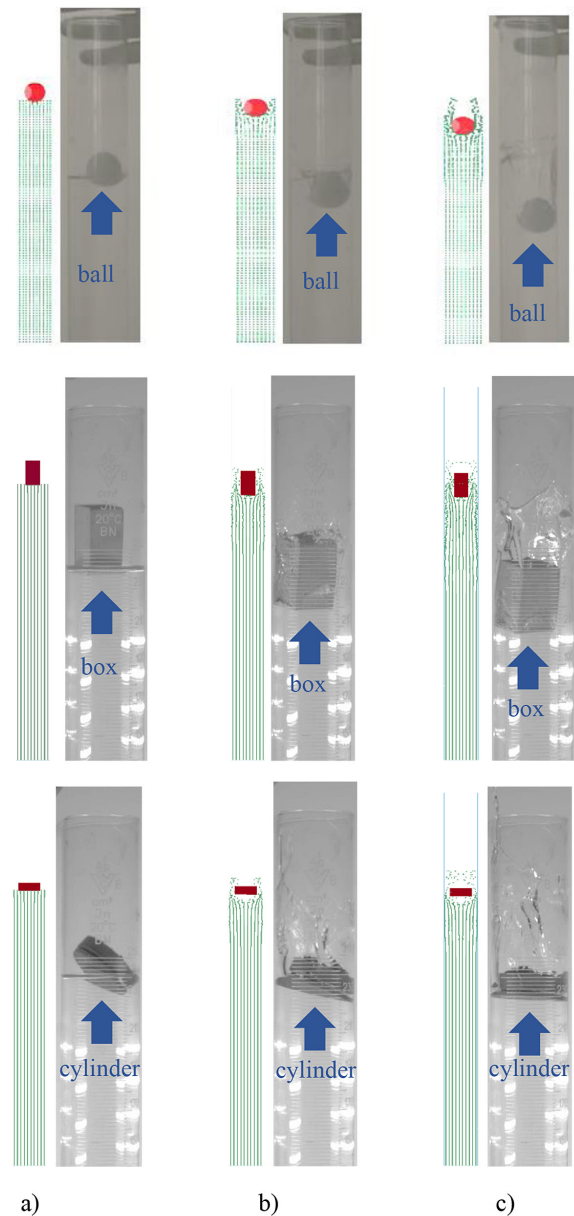


Figure 6. Comparison of the results of the impact of simulation of the bodies with water with images from a high-speed camera: a) at the moment of impact with the water, b) 25 ms after impact, c) 50 ms after impact

that the cylinder in the experiment hits the water differently than in the numerical simulation. Additionally, the measurement of the final immersion of the bodies, when its velocity was 0 m/s, in the experimental tests matched the results of calculations carried out using the SPH and ALE methods. The depth of bodies was shown in Table 3.

Based on experimental verification, it was found that the proposed methodology for performing calculations in the field of solid-water collision is appropriate, and both the SPH and ALE methods can be used to perform this type of simulation. The percentage differences in the

Table 3. Results of the depth of bodies

The immersion depth of bodies [cm]			
Shape	SPH simulation	ALE simulation	Experiment
Ball	3.58	3.49	3.67 ± 0.1
Box	3.17	3.15	3.25 ± 0.1
Cylinder	0.98	0.92	1.10 ± 0.1

immersion of bodies at the velocity of 0 m/s between the experiment and the SPH and ALE methods are between 2.45% and 4.63% in case of ball, respectively, in the case of box are 2.45% for SPH and 3.07% for ALE. For cylinder there were higher differences between the experiment and the SPH and ALE methods and the values are 10.9% and 16.3% respectively.

Taking into account the size of the screen plane model that will be used in the next calculation stage and the computing power necessary to perform the calculations, it was decided that the ALE method would be used to analyze the WIG-craft landing on the water.

CALCULATIONS OF THE LANDING ON WATER OF THE UAV MODEL USING THE ALE METHOD

To estimate the loads that occur during the beginning of landing of the WIG-craft on the water, a computational model of the UAV structure was prepared. The calculations were carried out

using the ALE method and the results regarding the structure overloads were compared with the results of the calculations carried out according to the literature relations [21] and during the tests when using a model of a real object. During the tests, acceleration (Fig. 7) was measured during regular water landing (Fig. 8).

A strength analysis of selected aircraft components that were considered essential for the safe execution of water landing operations was also carried out.

Using the LS DYNA computing environment, an analysis of the water landing WIG-craft were carried out, the aircraft’s forward speed of 22 m/s and a vertical component of 3 m/s. The WIG-craft model was prepared based on 24 883 shell elements defined by the Belytschko-Tsay shell formula, with five integration points of thickness. The thicknesses of individual element groups were defined using the *SECTION_SHELL card.

The WIG-craft model was made with a span of 6 m and a length of 5.6 m. The modeled aircraft has a classic aerodynamic configuration, and the wings are solutions in the high-wing system

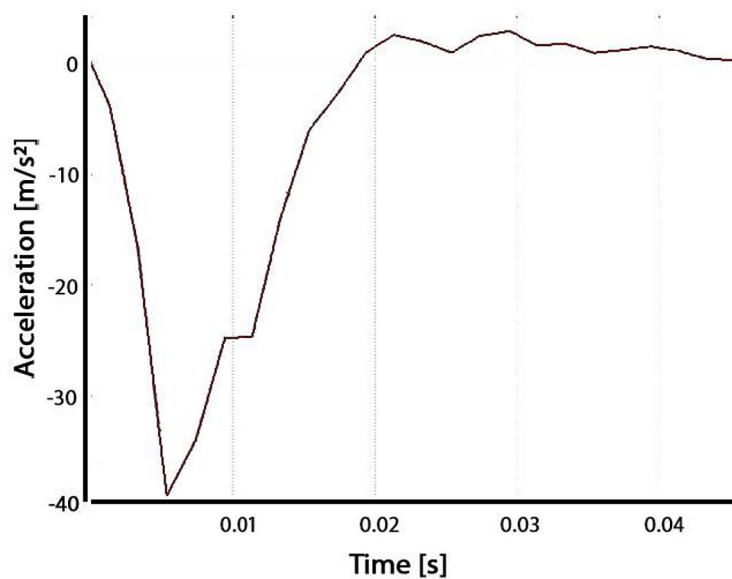


Figure 7. The acceleration $[\frac{m}{s^2}]$ measured during a regular water landing of a model of a WIG-craft

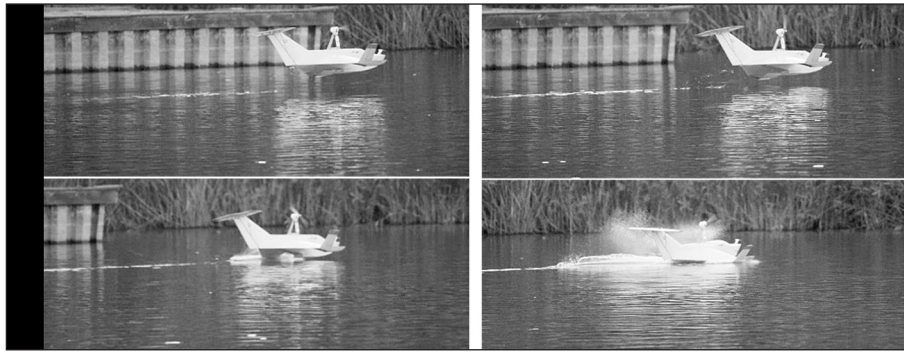


Figure 8. A sequence of photos of the regular water landing of a model of a WIG craft

mounted directly to the fuselage. At their end, there are auxiliary floats connected directly to the tail in the form of winglets. The wing has a negative sweep (-4.5°) together with a trailing edge sweep (-31.5°) shown in Figure 9.

For the needs of the analyzes, a monocoque solution was adopted for the construction of wings, empennage (vertical and horizontal) and winglets. On the other hand, for the main fuselage, which also serves as the main float, a semi-monocoque design solution was adopted with

skeleton elements in the form of seven frames spaced equally apart every 550 mm. A similar design system was adopted for the side floats, in which three frames were modeled evenly spaced along its length, every 600 mm. Additionally, the main fuselage was divided into two parts: the floating part and the upper part. The upper and lower parts of the fuselage were separated by a floor – Figure 10.

The vertical swept tail is mounted at an angle of 54° to the longitudinal axis of the aircraft,

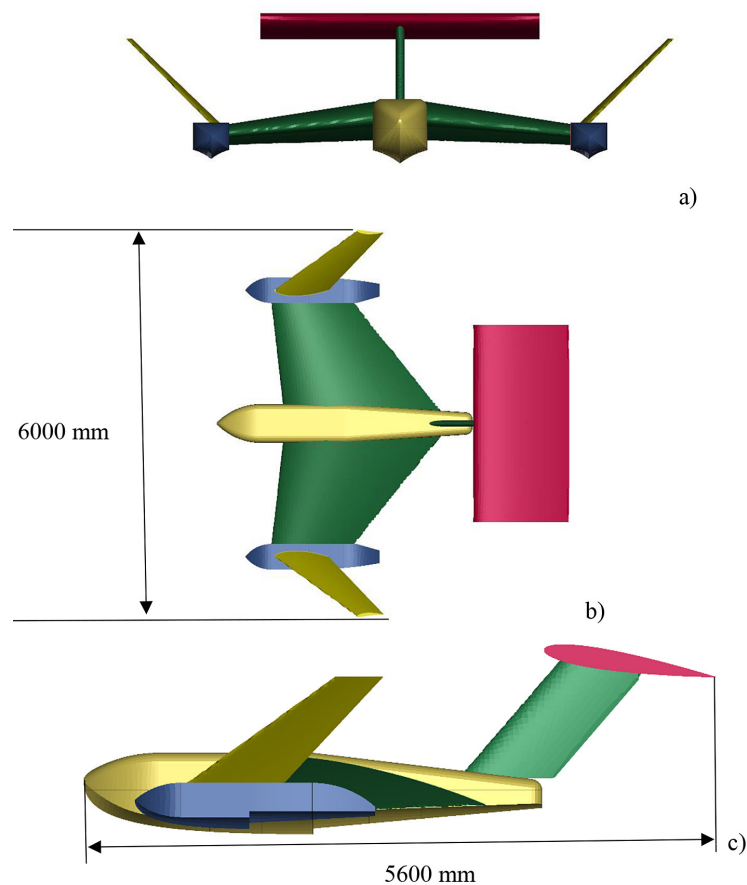


Figure 9. WIG-craft model a) front view, b) top view, c) side view

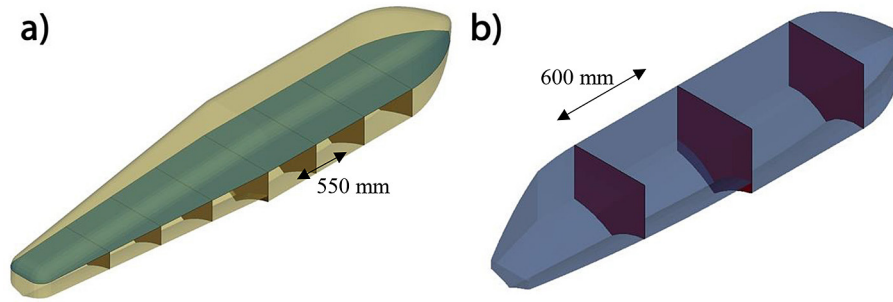


Figure 10. View of the internal structure of a) the fuselage, and b) the side float

while the horizontal tail is a straight tail. The swept winglets are mounted at an angle of 42° to the upper cover of the auxiliary float.

There were two WIG-craft calculations with different type structure materials. First, a calculation was made for structure material as polymer composite materials based on carbon fibers, CFRP (Carbon Fiber Reinforced Plastic), and second for aluminum alloy EN AW-2024T3. The parameters determined on the own material (composite) were adopted for modeling the material properties. The properties of the EN AW-2024T3 alloy material were taken from literature [23].

The composite was prepared based on a 160 g/m^2 carbon fabric (KORDCARBON, Czech Republic) and an epoxy resin with an aviation certificate L285 (MGS, Germany) with a density of 1.19 g/cm^3 mixed with a slow crosslinking

hardener H287 (MGS, Germany) in a 100:40 ratio. To obtain a composite with quasiisotropic properties, 13 layers of fabric layers were arranged according to the scheme $[[0, 30, 60]_4, 0]_T$. The composite was cured in two stages: in the first stage for 24 hours at 20°C using the vacuum bag technique and then at 80°C in a laboratory dryer (POL-EKO, Poland). A composite material with a thickness of $2.5 \pm 0.1 \text{ mm}$ was obtained. The stress-strain curve determined for this material was prepared on the MTS 809 test machine (MTS, USA) and using the Epsilon 3542-025M-025-HT2 extensometer (Epsilon, USA) – Figure 11. The parameters of the material produced are presented in Table 4 with material data of EN AW-2024T3 alloy.

Data on the thickness of individual structural elements are presented in Table 5. They were the same in both cases (CFRP and EN AW-2024T3).

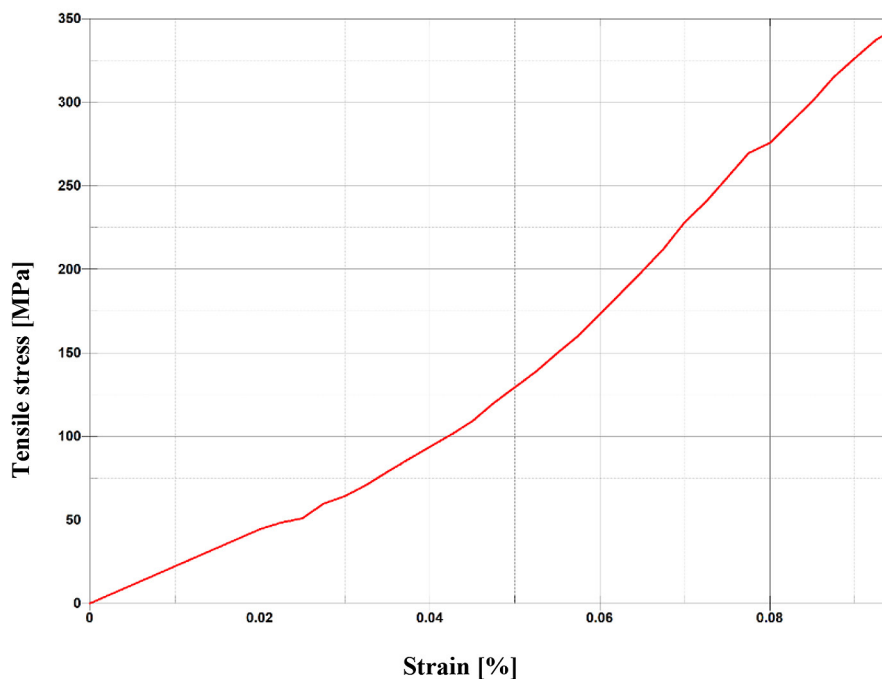


Figure 11. Tensile stress curve of the composite material

Table 4. Material data of CFRP and EN AW-2024T3 [23]

Parameter	CFRP	EN AW-2024T3
Density [kg/m ³]	1800	2780
Young's modulus [GPa]	39	73
Poisson's number	0.25	0.33
Yield point [MPa]	343	302
Ultimate strength [MPa]	343	447
Failure strain [%]	0.945	16.5

Table 5. Thicknesses of individual structural elements of the WIG-craft

Construction element	Thickness [mm]
Side float frames	2
Inner fuselage floor	2
Wings	1.5
Winglets	1
Fuselage frames	3
Vertical tail	1.5
Skin of the side floats	2
Horizontal tail	2
Fuselage skin	2.5

The total weight of the numerical models is 148 kg for CFRP structure, and 233 kg for EN AW-2024T3 structure.

For the purposes of performing the calculations, a water model was prepared in the shape of a cuboid with dimensions of 10 m in length, 7 m in width and 1.5 m in height, consisting of 105 000 identical solid elements – Figure 12.

To map the material properties of water, the ALE formula was used together with the definition of the water state equation using the *EOS_LINEAR_POLYNOMIAL card, which is presented in Table 1. The calculations were performed on a PC

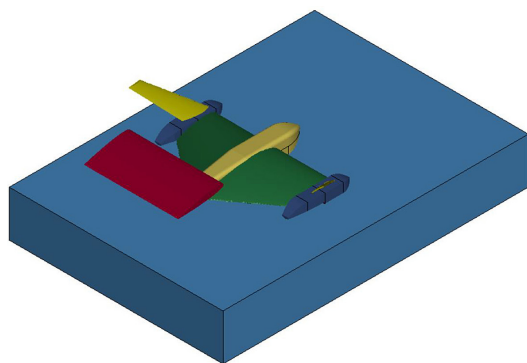


Figure 12. WIG-craft and water model at time $t = 0$ ms

workstation, and the calculation time was about 25 h. The analysis was completed without errors after 45 ms of simulation. According to the results of the calculation, the maximum overload value of the center of mass was 4.05 for the CFRP structure and 3.44 for EN AW-2024T3 structure. In Figure 13, the resultant acceleration of the center of mass are present for the composite (CFRP) and metal (EN AW-2024T3).

Based on numerical simulations, the largest acceleration for composite structure was 39.73 m/s² and for metal structure was 33.77 m/s². This is due to the fact that the metal structure deforms more than the composite one, and hence the lower resultant acceleration and overload values in the center of mass. During the tests, acceleration of real WIG-craft was measured, which has that same geometry and was built by composite materials. The same landing velocity was taken into account. The measured acceleration was made by a three-axial accelerometer, which was placed near by center of mass of WIG-craft (the difference in the the x-axis was about 0.3 m in direction of the tail). The largest measure acceleration in the real structure was about 39.84 m/s², which gives a difference in the obtained results calculated in the numerical simulation and the test landing about 0.2%.

For comparison, the maximum overload value obtained in the calculations was compared with the overload value determined analytically according to the relationship (13) presented in [21], where:

$$n_w = \frac{KV_{SO}^2}{\sqrt[3]{(\tan \beta)^2 m_{UAV}}} \quad (13)$$

where: n_w – resultant overload during water landing; K – design factor for seaplanes is 0.012; V_{SO} – resultant speed of the UAV at the moment of water landing; β – angle of spacing of the lower part of the float; m_{UAV} – UAV mass.

Based on the analytical estimate, the resultant overload during landing was 3.98. The difference

$$w = \frac{KV_{SO}^2}{\sqrt[3]{(\tan \beta)^2 m_{UAV}}}$$

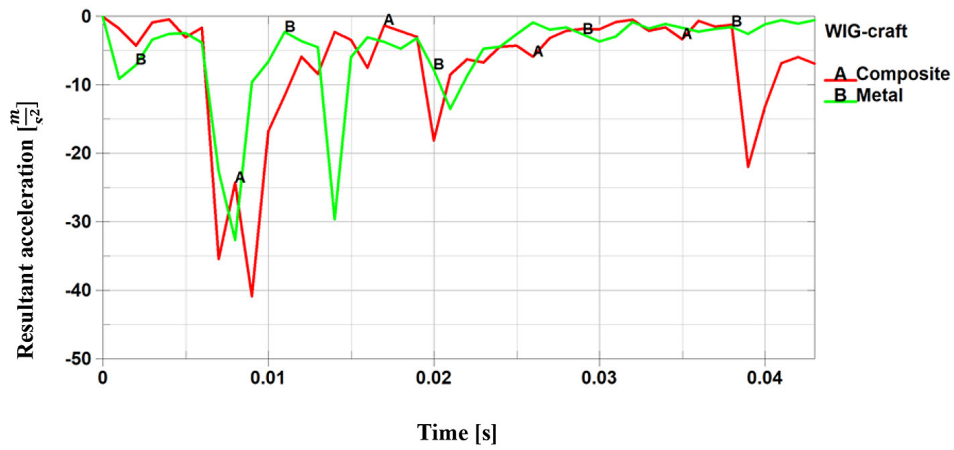


Figure 13. Resultant acceleration of the center of mass

in the obtained results calculated in the numerical simulation and analytically for the vertical overload occurring in the center of mass of the UAV was less than 2% for composite structure, and 10% for metal

structure. Based on numerical simulations, the stress distribution field according to the von Mises hypothesis was also obtained in the structural elements at the moment of landing (Fig. 14). Interactions

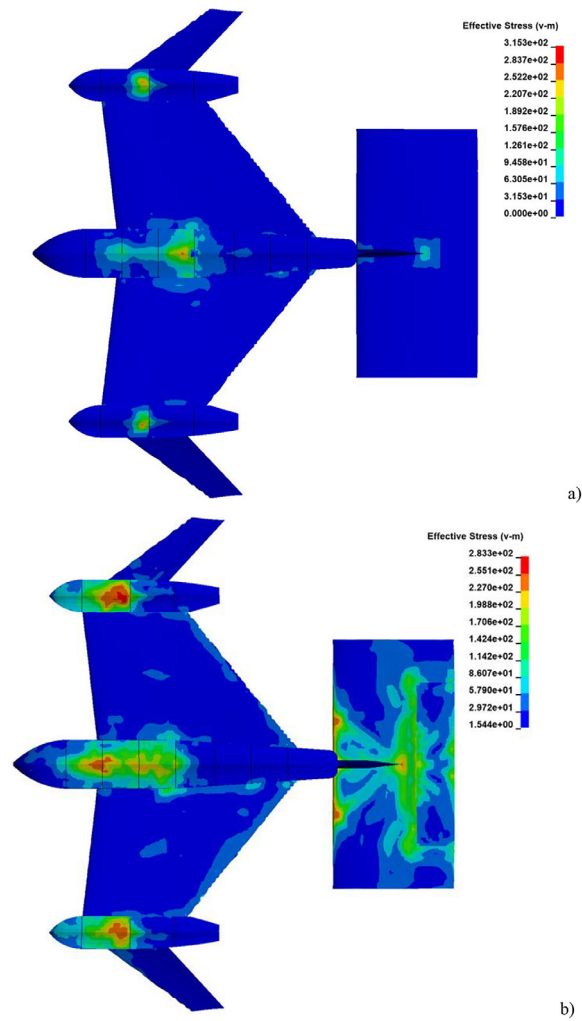


Figure 14. Distribution of stresses according to the von Mises hypothesis in the model at the moment of landing, a) composite structure, b) metal structure

between water and the aircraft related to the landing operation, assuming ideal conditions for this operation (including no waves, symmetrical loading of the structure), caused a complex stress state in the lower part of the fuselage, in which the highest stress values are equal to approximately 315 MPa for the composite structure and 270 MPa for metal structure. This stress value is lower than the ultimate strength in both cases, but the stress reserve of the structure is lower than the values recommended for aircrafts, for which the safety factors of the structure should be equal to 1.5. Lower stress values occur on the lower skin of the side floats for the composite structure; the values are 252 MPa. But the highest stress values for the metal structure are in the side floats, and equal 283 MPa. Another place where the stress field increases values is the place where the vertical and horizontal tails connect. Maximum stress values are equal to 126 MPa for the composite structure. In the metal structure the stress distribution field according to the von Mises hypothesis was different from the composite structure. The highest stress values are at the leading edge of the horizontal tail; the values are 255 MPa.

CONCLUSIONS

Based on the calculations and analyzes performed, it was found that:

- using both methods, SPH and ALE, it is possible to perform numerical simulations of phenomena involving fluid-solid interaction. Such simulations can effectively supplement or replace expensive and difficult to implement full-scale experimental studies,
- the challenge when using the SPH method is the demand for the so-called computing power of the computing stations currently in use,
- on the basis of calculations, it was found that the permissible stresses in the material of the structure were not exceeded for the proposed structure, but the reserves related to the effort are insufficient. Therefore, in the next construction steps, both the skeleton and the aircraft's covering should be modernized,
- in the next calculation steps, it is also necessary to analyze cases of landing during waves and cases of asymmetric landing, e.g. with a tilt onto the side float.

The aim of further work will be to investigate the phenomenon of launching during the

occurrence of sea waves, to conduct experimental launching of WIG-craft structures using measuring devices such as strain gauges to obtain measurements of strains and stresses.

Acknowledgements

This research was funded by the National Center for Research and Development under the Program for State Defense and Security entitled "Development of modern, breakthrough technologies for state security and defense" under a codename "SZAFIR" – Competition No. 4/SZAFIR/2021, Project title: "Unmanned surface and air platform using the near-surface effect supporting the operations of Special Forces in maritime areas", Contract number: DOB-SZAFIR/01/B/036/04/2021 of December 20, 2022.

REFERENCES

1. Dharma D., Munir R., Siregar T.D.K. Interaction between fluid and solid body surfaces in fluid simulation using material-point method. School of Electrical Engineering and Informatics Institut Teknologi Bandung, Indonesia, 2018.
2. Smith F.T., Balta S., Liu K., and Johnson E.R. On dynamic interactions between body motion and fluid motion. University College London, London WC1E 6BT, UK, 2012.
3. Smith, F.T., Wilson, P.L. Fluid-body interactions: clashing, skimming, bouncing. *Phil. Trans. R. Soc. A*, 2011; 369, 3007–3024.
4. Cheng H., Chao F. Simulation of fluid-solid interaction on water ditching of an airplane by ale method. Department of Mechanics and Engineering Science, Fudan University, Shanghai 200433, China, 2011.
5. Chen J., Xiao T., Wang M., Lu Y. and Tong M. Numerical study of wave effect on aircraft water-landing performance. College of Aerospace Engineering, Nanjing University of Aeronautics and Astronautics, 2011.
6. von Karman T. The impact on seaplane floats during landing. Technical Report NACA TN-321, NACA, Washington, D. C. 1929.
7. Tien, C.M.T., Cong, D.N., Mai, D.N., et al. High-order fluid solver based on a combined compact integrated RBF approximation and its fluid structure interaction applications. *Comput. Fluids*, 2016; 131(5), 151–168.
8. Panagiotou, P.A., Ioannis, A., Neophytos, L., et al. FEM approach for diagnosis of induction machines' non-adjacent broken rotor bars by short time Fourier transform spectrogram. *J. Eng.*, 2019; 17, 4566–4570.

9. Peng, W., Wei, Q. Solving 2-D water entry problems with a CIP method and a parallel computing algorithm. *Mar. Syst. Ocean Technol.*, 2016; 11(1–2), 1–9.
10. Yang Y., Shao J. Numerical simulation of fluid–structure interaction with SPH method. College of Mechanical Engineering, Chongqing University of Technology, Chongqing 400054, People’s Republic of China, 2020.
11. Souli M., Sofiane Y. and Olovsson L. ALE and fluid/structure interaction in LS-DYNA. American Society of Mechanical Engineers, Pressure Vessels and Piping Division (Publication) PVP, 2004; (485): 181–189.
12. Hirt C.W., Nichols B.D. Volume of fluid (VOF) method for the dynamics of free boundaries. *J. Comput. Phys.*, 1981; 39(1), 201–225.
13. Tutt B.A., Taylor A.P. The use of LS-DYNA to simulate the water landing characteristics of space vehicles. 8th International LS-DYNA Users Conference Fluid/Structure. Dearborn, USA, 2004.
14. Hui S., Chi-Hua L. and You-Sheng H. Experimental research on the fluid-structure interaction in water entry of 2D elastic wedge. *Journal of Hydrodynamics, Ser. A*, 2003; 18(1), 104–109.
15. Fei L., Ling-Yu S. and Guang-Yue Z. et al. Simulation and experiment of cylinder shell structure dropping into water based on fluid structure interaction. *Journal of Beijing University of Aeronautics and Astronautics*, 2007; 33(9), 1117–1120.
16. Karen E.J., Yvonne T.F. Comparison of ALE and SPH simulations of vertical drop tests of a composite fuselage section into water. 10th International LS-DYNA Users Conference. Detroit, Michigan, USA, 2008.
17. Kellas, S., and Jackson, K.E. Multi-terrain vertical drop tests of a composite fuselage section. In: *Proceedings of the 64th AHS Forum*, Montreal, Canada, 2008.
18. *General Aviation Aircraft Design, Appendix 3C: Seaplane Design*.
19. Rojewski A., Bartoszewicz J. Numerical analysis of influence of the wing in ground effect on aircraft lift coefficient and on car downforce coefficient, *Journal of Mechanical and Transport Engineering* 2017; 69(2).
20. Wiriadidjaja S., Zhahir A., Mohamad Z.H., Razali S., Puaat A.A., Ahmad M.T. Wing-in-ground-effect craft: A case study in aerodynamics, *International Journal of Engineering & Technology*, 2018.
21. Karen E. Jackson, Jacob B. Putnam. Water ditching simulation of a Fokker F28 fellowship aircraft, National Institute of Aerospace, Hampton, Virginia, USA, 2020.
22. Bae D.M., Zakki A.F. Comparisons of multi material ALE and single material ALE in LS-DYNA for estimation of acceleration response of free-fall lifeboat. Department of Naval Architecture and Marine Systems Engineering, Pukyong National University, 2011.
23. Miturska-Baranska I., Rudawska A. and Doluk E. Influence of physical modification of the adhesive composition on the strength properties of aerospace aluminum alloy sheet adhesive joints, *MDPI Materials*, 2022.